OPEN ACCESS
Journal of Innovative Optical Health Sciences
Vol. 14, No. 5 (2021) 2142003 (13 pages)

DOI: 10.1142/S1793545821420037

World Scientific
www.worldscientific.com

Ex-vivo confocal Raman microspectroscopy of porcine skin with 633/785-NM laser excitation and optical clearing with glycerol/water/DMSO solution

Ali Jaafar[*,†,‡,§§], Malik H. Mahmood[*,†,§], Roman Holomb[*,¶], László Himics[*], Tamás Váczi[*], Anton Y. Sdobnov[‖,**], Valery V. Tuchin[‖,††,‡‡] and Miklós Veres[*]

[*]*Institute for Solid State Physics and Optics*
Wigner Research Centre for Physics
P.O. Box 49, H-1121 Budapest, Hungary

[†]*Institute of Physics, University of Szeged*
Dom ter 9, H-6720 Szeged, Hungary

[‡]*Ministry of Higher Education and Scientific Research*
Baghdad 10065, Iraq

[§]*Physiology Department, College of Medicine*
University of Misan, Al-Amarah, Misan 62001, Iraq

[¶]*Uzhhorod National University, Uzhhorod 88015*
Transcarpathia, Ukraine

[‖]*Science Medical Center, Saratov State University*
83 Astrakhanskaya Str., Saratov 410012, Russia

[**]*Optoelectronics and Measurement Techniques Laboratory*
University of Oulu, 90570 Oulu, Finland

[††]*Laboratory of Laser Diagnostics of Technical and Living Systems*
Institute of Precision Mechanics and Control
of the Russian Academy of Sciences
24 Rabochaya, Saratov 410028, Russia

[‡‡]*Interdisciplinary Laboratory of Biophotonics*
National Research Tomsk State University
36 Lenin Avenue, Tomsk 634050, Russia
[§§]*alijaafar@szfki.hu*

Received 19 March 2021
Accepted 5 May 2021
Published 31 May 2021

[§§]Corresponding author.

Confocal Raman microspectroscopy (CRM) with 633- and 785-nm excitation wavelengths combined with optical clearing (OC) technique was used for *ex-vivo* study of porcine skin in the Raman fingerprint region. The optical clearing has been performed on the skin samples by applying a mixture of glycerol and distilled water and a mixture of glycerol, distilled water and chemical penetration enhancer dimethyl sulfoxide (DMSO) during 30 min and 60 min of treatment. It was shown that the combined use of the optical clearing technique and CRM at 633 nm allowed one to preserve the high probing depth, signal-to-noise ratio and spectral resolution simultaneously. Comparing the effect of different optical clearing agents on porcine skin showed that an optical clearing agent containing chemical penetration enhancer provides higher optical clearing efficiency. Also, an increase in treatment time allows to improve the optical clearing efficiency of both optical clearing agents. As a result of optical clearing, the detection of the amide-III spectral region indicating well-distinguishable structural differences between the type-I and type-IV collagens has been improved.

Keywords: CRM; skin; collagen types I and IV; amide III; tissue optical clearing; glycerol; DMSO.

1. Introduction

In recent years, there has been increasing research interest in biomedical photonics, with the main focus on the development of *in-vivo* techniques and methods allowing for noninvasive skin disease diagnosis and monitoring of penetration and permeation of drugs and cosmetics into the skin as well as for the investigation of their action.[1,2] There are numerous noninvasive optical techniques, including but not limited to the confocal Raman microspectroscopy (CRM),[3–6] Raman spectroscopy (RS) and coherent anti-Stokes Raman spectroscopy (CARS),[4,7] optical coherence tomography (OCT),[8–10] multiphoton tomography (MPT),[11–14] including laser scanning microscopy (LSM),[15] fluorescence spectroscopy[16,17] and terahertz spectroscopy,[18,19] and other methods,[20,21] which have been successfully implemented *in vitro* and *in vivo* for tissue physiological evaluation and diagnosis of skin pathophysiology.[22] Among the mentioned optical techniques, CRM takes a special place. The effect of Raman scattering has been discovered in 1928.[23] In general, this effect can be described using the quantum theory. In this way, the interaction of photons of emitted light with tissue molecules leads to photon scattering. So, CRM provides information on the molecular structure of observed tissue based on the detection of inelastically scattered light during the exchange of rotational and vibrational energies between emitted light and tissue molecules. By recording the spectral distribution and intensity of the Raman-scattered photons, the information on the chemical bonds present in a tissue can be obtained, since the amount of scattering is proportional to the amount of bonds in molecules. In fact, the Raman spectrum of tissue can be considered as its unique molecular fingerprint containing information about tissue chemical composition. Indeed, the Raman peaks give information about the bonding configuration of functional groups, and the molecule can be identified from a combination of Raman bands or based on previous data on a given sample system. In this way, the analysis of Raman spectra allows obtaining information about the biochemical properties of the observed tissue.[24] Furthermore, even slightest changes in tissue composition lead to changes in Raman peaks' position and intensity; CRM can be used as an effective tool for early diagnosis of skin diseases and monitoring age-related changes. In the case of the skin, the recorded Raman spectrum represents fingerprint signatures for the chemical composition of various tissue components such as collagen, blood, proteins, lipids and nucleic acids.[25]

The main limitation to receive a signal from the deep region of skin by CRM, as well as by all the above-mentioned optical imaging techniques, is related to the turbid character of the biological cells, which are the building blocks of different skin layers. All these layers (epidermis, dermis and hypodermis) are characterized by high light scattering and absorption properties. Moreover, the deeper biological tissues, such as dermis and hypodermis, have 10–100 times higher scattering coefficients comparing to their absorption ones.[26,27] Generally, the scanning depth for an optical imaging technique in practice does not exceed 200 μm for most biological tissues, except in the case of the OCT

technique, where the signal can be detected at several millimeters at comparatively poor spatial resolution.[28] In the case of skin, the probing depth for optical methods is even less, due to the strong scattering of the *stratum corneum* (SC) and the epidermis (limited to approximately 100 μm).[29]

With the main aim to increase the penetration efficiency of excitation light into the deep layers of skin regions and improve the scanning depth for optical spectroscopic and imaging methods, the so-called optical clearing (OC) technique was developed in the nineties of the last century. The OC method allows one to control the optical properties of the biological tissues, particularly by significantly reducing the light-scattering properties of skin tissues. It was successfully used to increase the probing depths of optical imaging techniques in different biological tissues and to enhance the contrast of the optical images, as well as to improve the light-focusing ability, and increase the spatial resolution for numerous noninvasive optical diagnostic methods.[26,30–32] The mechanisms of interaction of the optical clearing agents (OCAs) with biological tissues are not completely understood yet. However, the majority of research works agree that there are three main mechanisms that tend to describe the processes during OC.[33] The first one is based on matching the refractive indices of different components within the biological tissues and tissue liquids. It is initiated by the diffusion of OCA into the tissue.[26,32–40] The second mechanism is related to biological tissue dehydration caused by an OCA's hyperosmolarity,[26,35,36,40–42] while the third is based on the molecular interactions of exogenous chemical agents that lead to the dissociation of collagen fibers.[40,43–46] A more detailed description of the mechanisms of interaction between the biological tissues and OCAs is available in the literature.[29,47]

Nowadays, a large variety of optical imaging techniques, such as OCT,[36,39,48] 3D confocal microscopy,[49] polarized microscopies,[50] RS[51,52] and CRM,[25,53,54] are used in combination with different optical clearing agents like glucose,[35,55] dimethyl sulfoxide (DMSO),[40] glycerol,[52,56] PEG 300,[52] PEG 400 and thiazone,[39] Omnipaque-300 (iohexol),[52] Sca*l*eS[38] and Sca*l*e.[37] It was discovered previously that combined application of OC technique and CRM allows to increase the probing depth up to 400 μm.[25] Glycerol is one of the most frequently employed OCAs due to its biocompatibility, pharmacokinetics, a high index of refraction matching and dehydration action. For these reasons, we used glycerol as a major component of OCAs in our investigation to enhance the probing depth of porcine skin by CRM.

Despite a large number of research articles, very little attention has been paid to study the role of OCAs for different tissues. Moreover, there is no relevant information on the effect of exposure time and other parameters like physical penetration depth into the tissue when OCAs are combined with different chemical enhancers. These agents are generally considered nontoxic but applying at long exposure time and high concentration can result in negative effects on the skin, like extreme tissue compression, local hemostasis and in some cases, even tissue necrosis. Some OCAs act as chemical permeability enhancers and cause alterations in the skin morphology due to a dissociation of the collagen fibers.[8,45,57,58] Thus, it is critically important to avoid or reduce the negative effect and find the most efficient agent, the safest concentration and the optimal exposure time, especially for *in-vivo* imaging of living tissues.

It was demonstrated that DMSO, applied on human skin, provides a faster, more effective and safer optical clearing process, during which the conformation of keratin in the SC changes from α-helical to β-sheet. Moreover, it was observed that the DMSO causes an altering effect on the SC lipid organization by transforming the predominant all-trans gel phase to the trans-gauche liquid crystalline phase that boosts the penetration of additional substances into the skin tissues.[59]

CRM is an efficient tool to probe the chemical bonding structure of different substances, including the biological samples. Unfortunately, the information obtained by this technique is mainly derived from the surface or near-surface regions. This is especially true for skin tissues that are usually characterized by a high scattering and/or a high absorption cross-section. The physical reason behind that is a broad variety of refraction indices related to the different tissues and cellular components. It was found that the penetration depth for visible and near-infrared light, usually used by Raman microscopy methods, is limited to the epidermis.[29] In this study, we present an investigation of OCAs' influence on probing depth using porcine skin with CRM assessment. The influence of glycerol and water mixture has been compared to the influence of a mixture of glycerol, water and DMSO

(penetration enhancer). The influence of both agents on Raman spectra and intensities of principal skin peaks has been investigated by CRM systems using 633-nm and 785-nm excitations.

2. Materials and Methods

2.1. *Reagents and sample preparation*

Glycerol was chosen for this study as the most commonly used and effective OCA for application to the skin due to its biocompatibility, pharmacokinetics and high index of refraction matching ($n = 1.47$),[60,61] thus, glycerol of 99% purity (purchased from the Sigma Aldrich, Ltd.) was used for our investigations. The efficiency of OC process depends on the type and concentration of OCAs as well as the applied exposure time. Previously, it was shown that low concentrations of glycerol could not provide sufficient OC while pure glycerol has limited penetration ability in skin due to its high viscosity. It was discovered that ≈70–80% glycerol in water solutions provides the fastest and most effective OC.[62] Thus, in this study the mixtures of 75% glycerol + 25% distilled water and 75% glycerol + 20% distilled water + 5% DMSO have been used as OCAs, the refractive indices for these solutions were $n = 1.437$ and 1.449, respectively. DMSO was used as the penetration enhancer, which reduces the barrier function of *stratum corneum* and also acts as OCA by itself.[56] In general, SC significantly slows down the penetration of OCA into the deeper layers of skin. The application of penetration enhancers can significantly increase OC speed and efficiency.

To study the optical clearing effect, fresh porcine ear skin was chosen as a model of the human skin. The porcine skin is an *ex-vivo* human skin model because it is morphologically, histologically and immunohistochemically similar to the human one.[63–66] However, the SC of human skin *in-vivo* experiments has a higher barrier function compared to the porcine one, which was recently determined by *ex-vivo* investigation applying the CRM technique.[67]

Four fresh porcine ears skin were obtained from a local accredited abattoir (Budapest, Hungary). Before the investigation, the skins were washed and cleaned out with cold running water, and then the remaining water was removed with a paper towel. To additionally increase OCAs' penetration through the skin, it was shaved to remove the remaining hair, and then 20 tapes were successively pressed onto the skin and removed. The tape stripping was followed by a defatting process by placing the sample in pure ethanol for 5 s. The tissue samples of $1 \times 1\text{-cm}^2$ size and approximately 1.2-mm thickness were manually sliced from the porcine ear with a scalpel and stored at 5°C for no longer than two days. Prior to the experiments, the skin samples were left for 30 min in an air-conditioned laboratory with a temperature of 20 ± 1°C that allowed them to equilibrate. Finally, the skin samples were placed in Petri dishes filled with the prepared OCAs for 30 min and 60 min. Skin without the optical clearing agent treatment (i.e., untreated skin) was used as a control sample. It should be noted that while both the epidermal and dermal sides of the samples were in contact with the OCAs, the applied exposure times, even in 60-min case, were not enough for the OCAs to penetrate through all skin layers from the dermal and epidermal sides.[62,68] All CRM measurements were performed by placing the skin samples on silicon substrates for easier handling and examination through the epidermis.

2.2. *Confocal Raman microspectroscopy*

Raman spectra were recorded in the backscattered geometry and confocal mode by using a Renishaw (UK) in Via Raman microscope. To obtain the depth (Z) profile of porcine skin, samples were placed on a computer-controlled three-axis motorized stage which allows the vertical movements of the sample with micrometer resolution; 633-nm and 785-nm laser sources were used separately for the measurements with 1800-g/mm and 1200-g/mm gratings with spatial resolutions of 0.77 μm and 0.95 μm and spot sizes of 1.5 μm and 1.9 μm, respectively. The laser beam was focused on the sample by a 50× objective and the Raman signal was also collected with it. To prevent the tissue damage, the delivered laser power on the sample surface was kept at 10 mW and 50 mW for 633 nm and 785 nm, respectively. Raman spectra were collected with 5 s of exposure time at four different spots on each sample. In this case, the low dose-dependent fluorescent photobleaching in the dermis and epidermis has no significant contribution to the Raman peak intensities.[69] Before measurements, OCAs were removed from the surface of sample

using a paper towel. All spectra were recorded and analyzed in the wavenumber region from 620 cm^{-1} to 1750 cm^{-1}. Before the Raman measurements, the system was spectrally calibrated using the 520-cm^{-1} Raman band of a silicon crystal. All recorded spectra from each sample were averaged, then processed and analyzed using the Spectragryph software (Savitzky–Golay smoothing with a third-order polynomial and an interval of 16 and baseline correction using a polynomial function).[70]

3. Results and Discussion

Figure 1 shows the examples of experimentally recorded Raman spectra of the untreated skin sample probed at different depths (from 0 μm to 240 μm) with 40-μm step size for different excitation wavelengths of 633 nm and 785 nm.

The principal Raman peaks of skin are located at 937 cm^{-1} (C–C stretch backbone), 1003 cm^{-1} (phenylalanine/urea), 1246 cm^{-1} (amide III), 1271 cm^{-1} (amide III), 1426 cm^{-1} (C–C stretching vibrations) and 1665 cm^{-1} (amide-I band) at a depth of 0 μm.[71] It is clearly seen in Fig. 2 that the intensity of Raman peaks related to the skin monotonically drops down with increasing the probing depth for both 633-nm and 785-nm excitations. However, it is seen that the intensity of Raman peaks for 633 nm decreases faster comparing to 785 nm. Moreover, Raman spectra obtained with 633-nm excitation are noisier. In fact, some principal Raman peaks cannot be resolved from noise at 80–120-μm depth for 633 nm, while for 785 nm, the same peaks can be resolved even at 160-μm depth. The decrease of the intensities of the observed peaks can be explained by the lower number of both probing and detected photons caused by high scattering and absorption properties of the skin tissue. Due to the cellular and subcellular structures with varying refraction indices fewer photons can reach the deeper-lying skin regions and at the same time, less Raman-backscattered photons can be detected from there, as well.

It is important to notice that the 633-nm and 785-nm laser sources used for Raman measurements both have their own benefits and drawbacks. At first, the light of different wavelengths has different penetration abilities in the skin. So, the use of 785-nm light source provides higher probing depth since more photons can penetrate to deeper skin layers. Second, due to the pigmented nature of skin, fluorescence can appear in the specimen.[72] In general, a laser with a shorter wavelength penetrating the skin layer more severe signal attenuation leading to decreased Raman signal intensity comparing to an excitation source of longer wavelength.[73] Thus, the Raman peaks in the fingerprint region can be overlapped by a high-fluorescence signal with a 633-nm laser. However, the use of 633-nm light

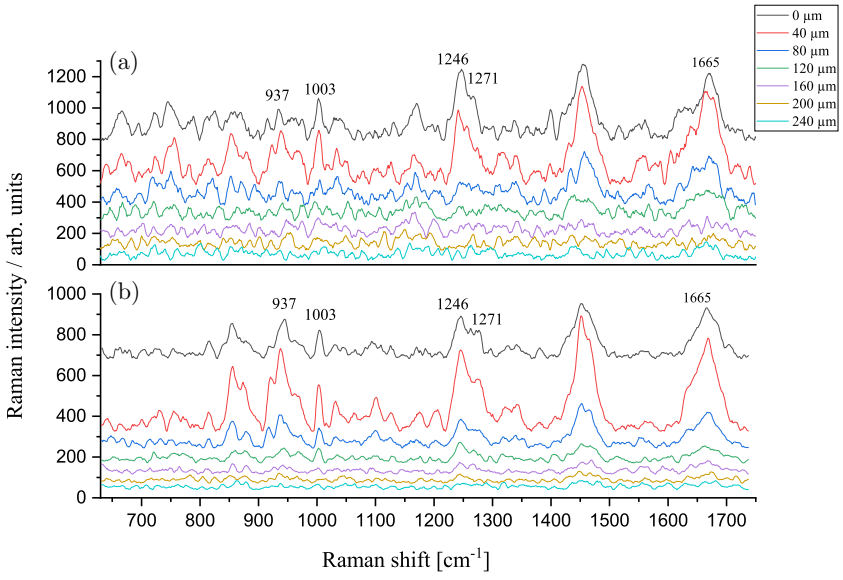

Fig. 1. Evolution of untreated porcine ear skin's Raman spectra from the depth of 0 μm to 240 μm in the fingerprint region (from 630 cm^{-1} to 1750 cm^{-1}) recorded with (a) 633-nm and (b) 785-nm laser excitations. The spectra were offset along the ordinate for clarity of presentation.

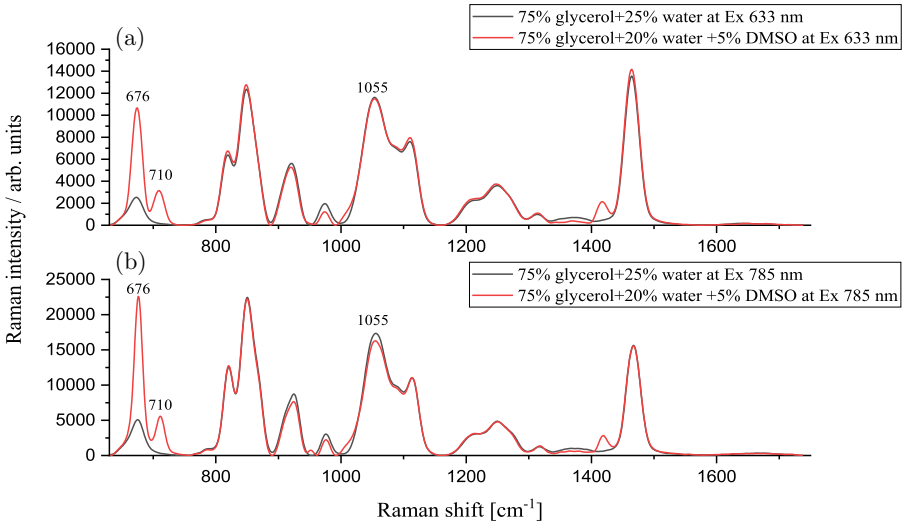

Fig. 2. Raman spectra of 75% glycerol+20% distilled water + 5% DMSO and 75% glycerol + 25% distilled water obtained with (a) 633-nm and (b) 785-nm excitations.

source can provide two important benefits: the bigger amplitude of the Raman signal and better spectral resolution, allowing for more precise analysis of skin molecular composition compared to the 785 nm. Additionally, the Raman intensity is inversely proportional to the fourth order of the excitation wavelength. Therefore, shorter excitation may be suitable to enhance the sensitivity. Moreover, 633-nm laser excitation was selected because quantum efficiency (sensitivity) of the CCD detectors' response is highly decreased in the near-infrared excitation leading to weaker Raman scattering efficiency. CCD efficiency rapidly decreases for high wavenumbers which are important for the evaluation of tissue water content and lipid characterization.[54,74] The maximum sensitivity of CCD detector at 633 nm allows to cover both low and high wavenumbers. At the same time, as it was shown before, 785 nm has a higher penetration ability in the skin. In this way, the application of OC technique with CRM using 633-nm light source will allow providing both high probing depth and spectral resolution for skin measurements.

In our investigation, we used glycerol and DMSO as OCAs for their biocompatibility and pharmacokinetics make them acceptable for the treatment of skin; in addition, they have different penetration characteristics in the skin layer, the diffusion rate of DMSO is faster than glycerol.[56] Figure 2 shows the Raman spectra of OCAs at 633-nm and 785-nm excitations. The main Raman peaks of glycerol are located at 1055 cm^{-1} and for DMSO markedly a strong doublet at 676 cm^{-1} and 710 cm^{-1}, assigned to symmetric and asymmetric υ (CSC) modes, respectively.

To investigate the influence of OC on the quality of the Raman spectra from deeper skin layers, a comparison of Raman spectra of untreated and OCA-treated porcine ear skin has been performed for both excitation light sources. Figures 3 and 4 show examples of depth-dependent Raman spectra of untreated skin and the skin after OCAs application for 30 min and 60 min for the 633-nm and 785-nm excitations, respectively. In general, due to the limited penetration ability of light into biological tissues, the intensities of the Raman spectrum decreased with the increased depth of measurement of untreated porcine skin. At depths of about 120 μm and 160 μm, the peaks were highly weakened at 1003, 1246 and 1271 cm^{-1} and overlaid by fluorescence background. It can be seen that after application of OCAs the intensities of the principal skin Raman peaks, as well as the signal-to-noise ratio, are increased in deeper skin regions for both 633-nm and 785-nm excitations. The intensities of principal skin Raman bands at 1003, 1246 and 1271 cm^{-1} for 633 nm are increased and became clearly revisable from noise after OCAs application for both 30 min and 60 min even at 240-μm depth. Also, longer treatment with OCAs leads to better effect. This means that the application of optical clearing technique with CRM using 633-nm light source allows achieving similar or even higher probing depth and quality of Raman spectra

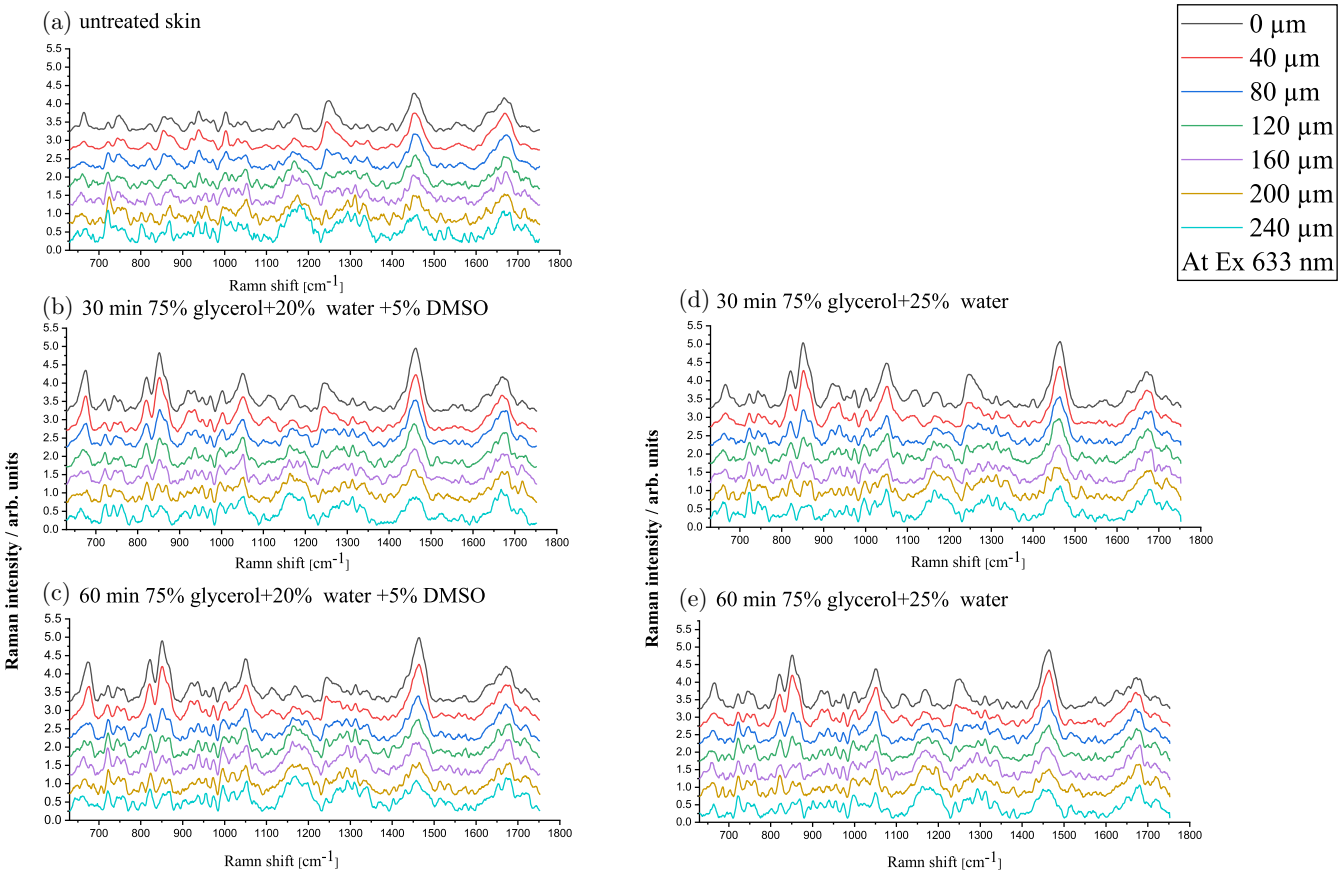

Fig. 3. Evolution of averaged Raman spectra from porcine ear skin from the depth of 0 μm to 240 μm in the fingerprint region (from 630 cm^{-1} to 1750 cm^{-1}) recorded with 633-nm laser excitation at 30 min and 60 min. (a) Untreated skin, (b), (c) skin treated with 75% glycerol + 20% distilled water + 5% DMSO and (d), (e) skin treated with 75% glycerol + 25% distilled water. The spectra were normalized from 1590 cm^{-1} to 1750 cm^{-1} and offset along the ordinate for clarity of presentation.

comparing to CRM using 785-nm light source without optical clearing. Thus, combined use of OC technique with CRM at shorter wavelength simultaneously provides high probing depth, signal-to-noise ratio and spectral resolution for skin measurements. The principal peaks for both OCAs can be resolved at Raman spectra at all depths after 30-min and 60-min treatments, meaning that both OCAs penetrated to all observed depths during the experiment.

In order to allow direct comparison of OC results at different skin depths, the skin spectra were first baseline corrected and normalized on the amide-I band (from 1590 cm^{-1} to 1750 cm^{-1}).[54,75,76] It is important to notice that the normalization on the amide-I band can be not fully correct for 40-μm depth. This can be due to the fact that this depth corresponds to *stratum spinosum* layer, which is protein-deficient in comparison with the SC, which is rich in keratin and to the dermis, which is rich in collagen I, collagen III and elastin.[14]

OCA application leads to flux of water from skin due to strong tissue dehydration and simultaneous penetration of OCA into tissue resulting in refractive index matching between agent and tissue. These processes, as well as tape-stripping and defatting procedures applied to skin samples before measurements, can lead to decreased backscattering at the upper layers of the SC. Thus, more exciting light could reach deeper tissue layers (photon penetration). As expected, the Raman spectrum of deep targeted regions could be investigated. In the previous studies, it was also demonstrated that the application of glycerol on porcine ear skins could efficiently improve the Raman-to-fluorescence ratio and signal contrast.[25,71]

Collagen types I and IV are the most prevailing constituents of the skin. Type-I collagen is the main molecular component in the dermis in high proportion (85–90%), while type-IV collagen is found in the basement membrane (composed of 10%).

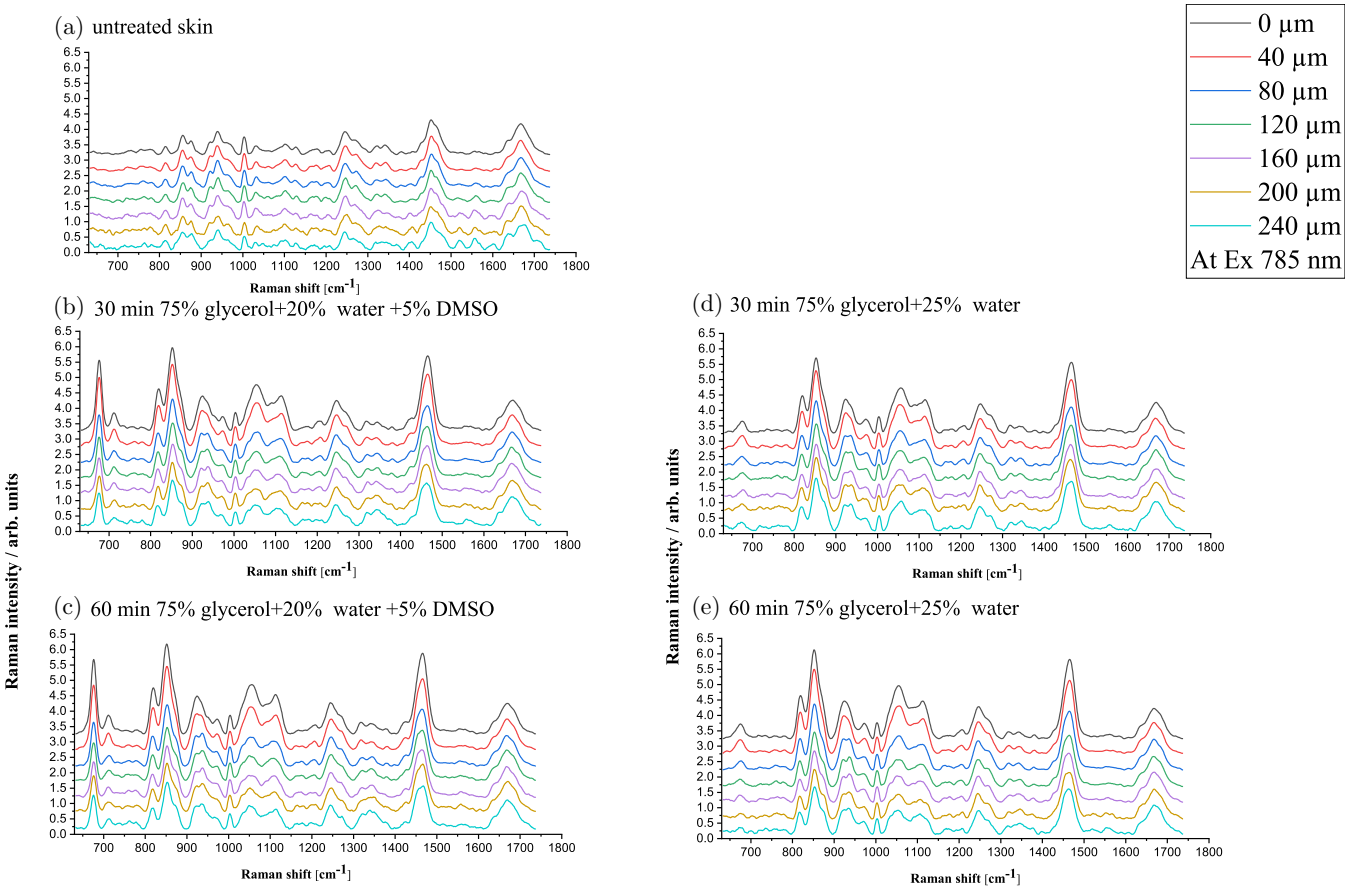

Fig. 4. Evolution of Raman spectra averages from porcine ear skin from the depth of 0 μm to 240 μm in the fingerprint region (from 630 cm^{-1} to 1750 cm^{-1}) recorded with 785-nm laser excitation at 30 min and 60 min. (a) Untreated skin, (b), (c) skin treated with 75% glycerol + 20% distilled water + 5% DMSO and (d), (e) skin treated with 75% glycerol + 25% distilled water. The spectra were normalized from 1590 cm^{-1} to 1750 cm^{-1} and offset along the ordinate for clarity of presentation.

These proteins are strongly altered during chronological skin ageing or cancer progression. The application of OC can significantly increase the quality of collagen structural alterations monitoring using CRM that is important for dermatological research. The amide-III region presents considerable differences between collagen types I and IV as well as the structural differences between epidermis, dermis and epidermis–dermis interface.[77] Raman intensity ratio I_{1271}/I_{1246} revealed the difference between both proteins in the distribution of proline-poor and proline-rich, respectively.[78]

To study the OCAs' effect on collagen types I and IV in porcine skin, the OC efficiencies for Raman peaks at 1246, 1271 and also 1003 cm^{-1} were analyzed for different depths.[79,80] The OC efficiency has been calculated as the I_{OC}/I ratio, where I_{OC} is the Raman intensity after the optical clearing agent treatment and I is the Raman intensity without treatment.[71] The depth-dependent efficiencies of OC for 1246-cm^{-1} proline-rich (non-polar), 1271-cm^{-1} proline-poor (polar) regions of the collagen and 1003-cm^{-1} peak after 30-min and 60-min applications of both OCAs are presented in Fig. 5. It is clearly seen that, in general, OC efficiency for both OCAs and light sources increased with treatment time. OC efficiency for 785 nm was higher than for 633 nm due to the better penetration ability. However, as it was mentioned before, the combined use of CRM and OC technique has a big potential for clinical measurements, since this approach allows to preserve simultaneously the high probing depth, signal-to-noise ratio and spectral resolution, which can be a key factor for the determination of early stage of skin diseases and monitoring of their treatment. The potential strengths of these bands can be associated with collagen dissociation at different treatments (with concentrated OCAs) or pathologies (malignancy for example), but because of a moderate glycerol concentration

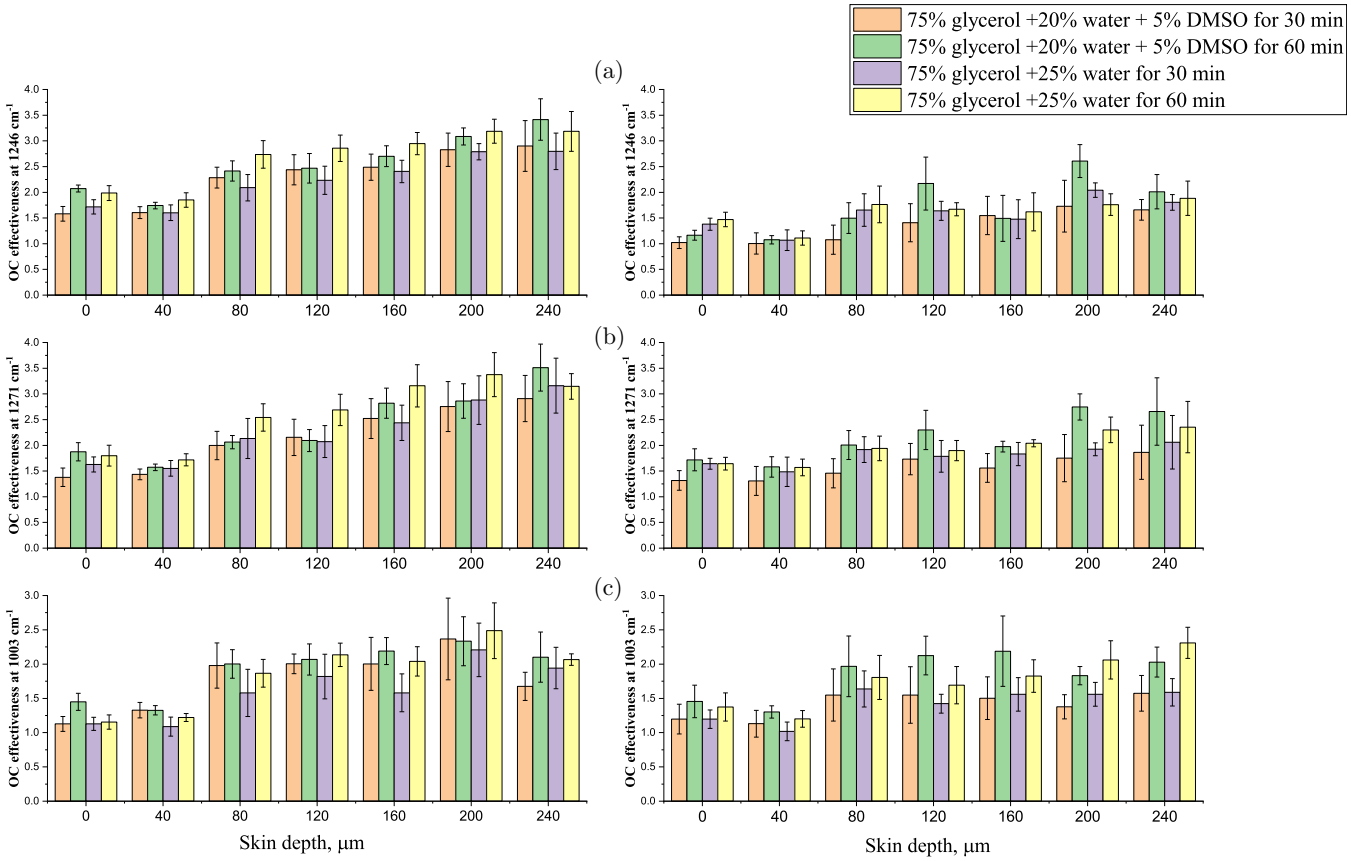

Fig. 5. Optical clearing effectiveness for the porcine skin treated by different OCAs for different exposure times of 30 min and 60 min for the Raman peaks at (a) 1246 cm^{-1}, (b) 1271-cm^{-1} amide-III region and (c) 1003-cm^{-1} phenylalanine/urea at different wavelengths (785 nm left column and 633 nm right column).

used in this study we did not see any impact associated with collagen dissociation, which is well fitted to study of collagen dissociation by nonlinear microscopy.[42]

Figure 5 shows the calculated values of the OC efficiency for the used OCAs. For 785 nm, the highest OC efficiency was achieved at 240-μm depth for the Raman peaks at 1246 cm^{-1} and 1271 cm^{-1} (3.4 and 3.5, respectively) after 60-min treatment with glycerol–water–DMSO solution. For 1003 cm^{-1}, the highest OC efficiency (2.4) was achieved at 200-μm depth after 60-min treatment with glycerol–water solution. In general, for both OCAs, increment of treatment time from 30 min to 60 min leads to an increase in OC efficiency at all depths. Adding 5% of DMSO to the OCA led to an increase of OC efficiency for the most observed depths. The maximum OC efficiency values increase was achieved at 240-μm depth for Raman peaks at 1246 cm^{-1} and 1271 cm^{-1} (from 3.1 to 3.4 and from 3.1 to 3.5, respectively). For 1003 cm^{-1}, the maximum OC efficiency increment (from 1.9 to 2.1) was achieved at 160 μm. The increment of OC efficiency for OCA containing DMSO can be described by the fact that DMSO is the penetration enhancer also acting as an effective topical OCA by itself.

For 633 nm, the highest optical clearing efficiency is achieved at 200-μm depth for Raman peaks at 1246 cm^{-1} and 1271 cm^{-1} (2.6 and 2.7, respectively) after 60-min treatment with glycerol–water–DMSO solution. For 1003 cm^{-1}, the highest OC efficiency (2.3) was achieved at 240-μm depth after 60-min treatment with glycerol–water solution. The same as for 785 nm, for 633 nm increment of treatment time resulted in OC efficiency growth. The maximum OC efficiency values increase was achieved after the application of OCA containing DMSO at 200-μm depth for Raman peaks at 1246 cm^{-1} and 1271 cm^{-1} (from 1.7 to 2.6 and from 2.3 to 2.5, respectively). For 1003 cm^{-1}, the maximum OC efficiency increment (from 1.6 to 2.2) was achieved at 160 μm.

The increase of intensities of collagen-related Raman peaks after treatment by both OCAs indicates that collagen fibers became arranged more compactly due to strong dehydration caused by glycerol.[71] The presented results are in a good agreement with previous results on the investigation of OCA influence on Raman spectra.[71] Since Raman signal is strongly dependent on elastic scattering,[81,82] strong OC can significantly reduce the intensity of Raman spectra. Thus, finding optimal cases for both good OC efficiency and Raman signal intensity is an important goal.[83] In this way, the application of the penetration enhancers on the skin, such as DMSO,[59] oleic acid[84] or hyaluronic acid,[85] can significantly improve the OC efficiency allowing to provide faster OC.

4. Conclusions

In this study, the OC technique has been applied for CRM measurements using 633-nm and 785-nm excitations. It was shown that the principal Raman peak intensities of skin are significantly increased at all observed depths after OCAs treatment for 30 min and 60 min for both the excitations. Application of OCA made accessible the deep layers of porcine skin for Raman investigations. Moreover, the combined use of OC technique and CRM at 633 nm allowed us to preserve simultaneously the high probing depth, signal-to-noise ratio and spectral resolution. It was shown that OCA containing penetration enhancers (glycerol–water–DMSO) could significantly increase the OC efficiency comparing to the OCA without penetration enhancers (glycerol–water). Also, both OCAs noticeably increased the intensity of the Raman bands at 1246, 1271 and 1003 cm^{-1}; the first two are related to proteins that are strongly changing during cancer progression or skin ageing and the latter plays a significant role for skin cancer detection. The addition of chemical enhancers to the OCA solutions provides faster and more efficient OC that potentially allows for the safer application of OCA to biological tissues.

Acknowledgments

This work was done under a scholarship of the Stipendium Hungaricum Scholarship Programme. This work was supported by the VEKOP-2.3.2-16-2016-00011 Grant, which is co-financed by the European Union and European Social Fund. Valery V. Tuchin was supported by RFBR Grant 18-52-16025 and the Grant of the Government of the Russian Federation (Registration No. 2020-220-08-2389). In addition, we would like to appreciate the support of Dr. Alaa Al-Halbosy for his technical support.

Conflict of Interest

The authors declare that there are no conflicts of interest relevant to this paper.

References

1. R. Schulz *et al.*, "Modeling of drug diffusion based on concentration profiles in healthy and damaged human skin," *Biophys. J.* **117**, 998–1008 (2019).
2. M. K. Matta *et al.*, "Effect of sunscreen application under maximal use conditions on plasma concentration of sunscreen active ingredients: A randomized clinical trial," *JAMA* **321**, 2082–2091 (2019).
3. C. Choe, J. Lademann, M. E. Darvin, "Analysis of human and porcine skin *in vivo*/*ex vivo* for penetration of selected oils by confocal Raman microscopy," *Skin Pharmacol. Physiol.* **28**, 318–330 (2015).
4. C. Krafft, J. Popp, "The many facets of Raman spectroscopy for biomedical analysis," *Anal. Bioanal. Chem.* **407**, 699–717 (2015).
5. S. Osseiran *et al.*, "Characterizing stratum corneum structure, barrier function, and chemical content of human skin with coherent Raman scattering imaging," *Biomed. Opt. Express* **9**, 6425–6443 (2018).
6. L. Zhang *et al.*, "Resolving water, proteins, and lipids from *in vivo* confocal Raman spectra of stratum corneum through a chemometric approach," *J. Vis. Exp.* **2019**(151), e60186 (2019).
7. R. Vyumvuhore *et al.*, "Raman spectroscopy: *In vivo* quick response code of skin physiological status," *J. Biomed. Opt.* **19**(11), 111603 (2014).
8. K. V. Berezin *et al.*, "Optical clearing of human skin using some monosaccharides *in vivo*," *Opt. Spectrosc.* **127**, 352–358 (2019).
9. J. Gallwas *et al.*, "Effect of optical clearing agents on optical coherence tomography images of cervical epithelium," *Lasers Med. Sci.* **30**, 517–525 (2015).
10. M. E. Shvachkina, D. D. Yakovlev, E. N. Lazareva, A. B. Pravdin, D. A. Yakovlev, "Monitoring of the process of immersion optical clearing of collagen bundles using optical coherence tomography," *Opt. Spectrosc.* **127**, 359–367 (2019).

11. M. Balu, H. Mikami, J. Hou, E. O. Potma, B. J. Tromberg, "Rapid mesoscale multiphoton microscopy of human skin," *Biomed. Opt. Express* **7**, 4375–4387 (2016).
12. K. Koenig, I. Riemann, "High-resolution multiphoton tomography of human skin with subcellular spatial resolution and picosecond time resolution," *J. Biomed. Opt.* **8**(3), 432–439 (2003).
13. E. A. Shirshin *et al.*, "*In vivo* optical imaging of the viable epidermis around the nailfold capillaries for the assessment of heart failure severity in humans," *J. Biophotonics* **11**(9), e201800066 (2018).
14. E. A. Shirshin *et al.*, "Two-photon autofluorescence lifetime imaging of human skin papillary dermis *in vivo*: Assessment of blood capillaries and structural proteins localization," *Sci. Rep.* **7**, 1171 (2017).
15. M. Rajadhyaksha, M. Grossman, D. Esterowitz, R. H. Webb, R. R. Anderson, "*In vivo* confocal scanning laser microscopy of human skin: Melanin provides strong contrast," *J. Invest. Dermatol.* **104**, 946–952 (1995).
16. V. H. Maciel, W. R. Correr, C. Kurachi, V. S. Bagnato, C. da Silva Souza, "Fluorescence spectroscopy as a tool to *in vivo* discrimination of distinctive skin disorders," *Photodiagnosis Photodyn. Ther.* **19**, 45–50 (2017).
17. I. Ferulova, A. Lihachev, J. Spigulis, "Photobleaching effects on *in vivo* skin autofluorescence lifetime," *J. Biomed. Opt.* **20**(5), 051031 (2015).
18. D. I. Ramos-Soto, A. K. Singh, E. Saucedo-Casas, E. Castro-Camus, M. Alfaro-Gomez, "Visualization of moisturizer effects in stratum corneum *in vitro* using THz spectroscopic imaging," *Appl. Opt.* **58**, 6581–6585 (2019).
19. K. I. Zaytsev *et al.*, "The progress and perspectives of terahertz technology for diagnosis of neoplasms: A review," *J. Opt. (United Kingdom)* **22**, 013001 (2020).
20. C. Merle, C. Laugel, P. Chaminade, A. Baillet-Guffroy, "Quantitative study of the stratum corneum lipid classes by normal phase liquid chromatography: Comparison between two universal detectors," *J. Liq. Chromatogr. Relat. Technol.* **33**, 629–644 (2010).
21. V. Kalchenko, I. Meglinski, A. Sdobnov, Y. Kuznetsov, A. Harmelin, "Combined laser speckle imaging and fluorescent intravital microscopy for monitoring acute vascular permeability reaction," *J. Biomed. Opt.* **24**(6), 060501 (2019).
22. B. Gotter, W. Faubel, R. H. H. Neubert, "Optical methods for measurements of skin penetration," *Skin Pharmacol. Physiol.* **21**, 156–165 (2008).
23. C. V. Raman, K. S. Krishnan, "A new type of secondary radiation," *Nature* **121**, 501–502 (1928).
24. A. Quatela, L. Miloudi, A. Tfayli, A. Baillet-Guffroy, "*In vivo* Raman microspectroscopy: Intra- and intersubject variability of stratum corneum spectral markers," *Skin Pharmacol. Physiol.* **29**, 102–109 (2016).
25. D. Huang *et al.*, "Optical clearing of porcine skin tissue *in vitro* studied by Raman microspectroscopy," *J. Biomed. Opt.* **17**, 015004 (2012).
26. V. V. Tuchin, *Tissue Optics: Light Scattering Methods and Instruments for Medical Diagnosis*, SPIE Press, Bellingham (2015).
27. E. Gratton, "Deeper tissue imaging with total detection," *Science* **331**, 1016–1017 (2011).
28. B. E. Bouma, G. J. Tearney, *Handbook of Optical Coherence Tomography*, Marcel Dekker, New York (2002).
29. A. Y. Sdobnov *et al.*, "Recent progress in tissue optical clearing for spectroscopic application," *Spectrochim. Acta A, Mol. Biomol. Spectrosc.* **197**, 216–229 (2018).
30. D. A. Boas, "A fundamental limitation of linearized algorithms for diffuse optical tomography," *Opt. Express* **1**, 404–413 (1997).
31. C. L. Smithpeter, A. K. Dunn, A. J. Welch, R. Richards-Kortum, "Penetration depth limits of *in vivo* confocal reflectance imaging," *Appl. Opt.* **37**, 2749–2754 (1998).
32. V. V. Tuchin, "Light propagation in tissues with controlled optical properties," *J. Biomed. Opt.* **2**, 401–417 (1997).
33. E. A. Genina, A. N. Bashkatov, V. V. Tuchin, "Tissue optical immersion clearing," *Expert Rev. Med. Devices* **7**, 825–842 (2010).
34. V. V. Tuchin, X. Xu, R. K. Wang, "Dynamic optical coherence tomography in studies of optical clearing, sedimentation, and aggregation of immersed blood," *Appl. Opt.* **41**, 258–271 (2002).
35. D. K. Tuchina *et al.*, "*Ex vivo* optical measurements of glucose diffusion kinetics in native and diabetic mouse skin," *J. Biophotonics* **8**, 332–346 (2015).
36. K. V. Larin *et al.*, "Optical clearing for OCT image enhancement and in-depth monitoring of molecular diffusion," *IEEE J. Sel. Top. Quantum Electron.* **18**, 1244–1259 (2012).
37. H. Hama *et al.*, "Sca*l*e: A chemical approach for fluorescence imaging and reconstruction of transparent mouse brain," *Nat. Neurosci.* **14**, 1481–1488 (2011).
38. H. Hama *et al.*, "Sca*l*eS: An optical clearing palette for biological imaging," *Nat. Neurosci.* **18**, 1518–1529 (2015).
39. D. Zhu, K. V. Larin, Q. Luo, V. V. Tuchin, "Recent progress in tissue optical clearing," *Laser Photonics Rev.* **7**, 732–757 (2013).

40. A. K. Bui *et al.*, "Revisiting optical clearing with dimethyl sulfoxide DMSO," *Lasers Surg. Med.* **41**, 142–148 (2009).
41. V. V. Tuchin, "A clear vision for laser diagnostics (review)," *IEEE J. Sel. Top. Quantum Electron.* **13**, 1621–1628 (2007).
42. X. Weny, Z. Maoy, Z. Han, V. V. Tuchin, D. Zhu, "*In vivo* skin optical clearing by glycerol solutions: Mechanism," *J. Biophotonics* **3**, 44–52 (2010).
43. J. Hirshburg, B. Choi, J. S. Nelson, A. T. Yeh, "Collagen solubility correlates with skin optical clearing," *J. Biomed. Opt.* **11**, 040501 (2006).
44. J. Hirshburg, B. Choi, J. S. Nelson, A. T. Yeh, "Correlation between collagen solubility and skin optical clearing using sugars," *Lasers Surg. Med.* **39**, 140–144 (2007).
45. J. M. Hirshburg, K. M. Ravikumar, W. Hwang, A. T. Yeh, "Molecular basis for optical clearing of collagenous tissues," *J. Biomed. Opt.* **15**, 055002 (2010).
46. A. T. Yeh, B. Choi, J. S. Nelson, B. J. Tromberg, "Reversible dissociation of collagen in tissues," *J. Invest. Dermatol.* **121**, 1332–1335 (2003).
47. L. M. C. Oliveira and V. V. Tuchin, *The Optical Clearing Method: A New Tool for Clinical Practice and Biomedical Engineering*, Springer International Publishing, Switzerland (2019).
48. X. Wen, S. L. Jacques, V. V. Tuchin, D. Zhu, "Enhanced optical clearing of skin *in vivo* and optical coherence tomography in-depth imaging," *J. Biomed. Opt.* **17**, 066022 (2012).
49. Y. Y. Fu, S. C. Tang, "Optical clearing facilitates integrated 3D visualization of mouse ileal microstructure and vascular network with high definition," *Microvasc. Res.* **80**, 512–521 (2010).
50. O. Nadiarnykh, P. J. Campagnola, "Retention of polarization signatures in SHG microscopy of scattering tissues through optical clearing," *Opt. Express* **17**, 5794–5806 (2009).
51. M. V. Schulmerich *et al.*, "Optical clearing in transcutaneous Raman spectroscopy of murine cortical bone tissue," *J. Biomed. Opt.* **13**, 021108 (2008).
52. Q. Lin, E. N. Lazareva, V. I. Kochubey, Y. Duan, V. V. Tuchin, "Kinetics of optical clearing of human skin studied *in vivo* using portable Raman spectroscopy," *Laser Phys. Lett.* **17**, 105601 (2020).
53. P. Liu *et al.*, "Discrimination of dimethyl sulphoxide diffusion coefficient in the process of optical clearing by confocal micro-Raman spectroscopy," *J. Biomed. Opt.* **18**, 020507 (2013).
54. A. Y. Sdobnov, M. E. Darvin, J. Schleusener, J. Lademann, V. V. Tuchin, "Hydrogen bound water profiles in the skin influenced by optical clearing molecular agents — Quantitative analysis using confocal Raman microscopy," *J. Biophotonics* **12**(5), e201800283 (2019), doi: 10.1002/jbio.201800283.
55. K. V. Larin, V. V. Tuchin, "Functional imaging and assessment of the glucose diffusion rate in epithelial tissues in optical coherence tomography," *Quantum Electron.* **38**, 551–556 (2008).
56. J. Jiang, M. Boese, P. Turner, R. K. Wang, "Penetration kinetics of dimethyl sulphoxide and glycerol in dynamic optical clearing of porcine skin tissue *in vitro* studied by Fourier transform infrared spectroscopic imaging," *J. Biomed. Opt.* **13**, 021105 (2008).
57. N. J. Yang, M. J. Hinner, "Getting across the cell membrane: An overview for small molecules, peptides, and proteins," *Methods Mol. Biol.* **1266**, 29–53 (2015).
58. S. R. Utz, V. V. Tuchin, E. M. Galkina, "The dynamics of some human skin biophysical parameters in the process of optical clearing after hyperosmotic solutions topical application," *Vestn. Dermatol. Venerol.* **91**(4), 60–68 (2015).
59. P. J. Caspers *et al.*, "Monitoring the penetration enhancer dimethyl sulfoxide in human stratum corneum *in vivo* by confocal Raman spectroscopy," *Pharm. Res.* **19**, 1577–1580 (2002).
60. M. H. Khan *et al.*, "Optical clearing of *in vivo* human skin: Implications for light-based diagnostic imaging and therapeutics," *Lasers Surg. Med.* **34**, 83–85 (2004).
61. V. Genin *et al.*, "*Ex vivo* investigation of glycerol diffusion in skin tissue," *J. Biomed. Photonics Eng.* **2**, 010303-1–010303-5 (2016).
62. A. Sdobnov, M. E. Darvin, J. Lademann, V. V. Tuchin, "A comparative study of *ex vivo* skin optical clearing using two-photon microscopy," *J. Biophotonics* **10**, 1115–1123 (2017).
63. S. Debeer *et al.*, "Comparative histology and immunohistochemistry of porcine versus human skin," *Eur. J. Dermatol.* **23**, 456–466 (2013).
64. S. Mangelsdorf, T. Vergou, W. Sterry, J. Lademann, A. Patzelt, "Comparative study of hair follicle morphology in eight mammalian species and humans," *Ski. Res. Technol.* **20**, 147–154 (2014).
65. M. E. Darvin *et al.*, "Comparison of *in vivo* and *ex vivo* laser scanning microscopy and multiphoton tomography application for human and porcine skin imaging," *Quantum Electron.* **44**, 646–651 (2014).
66. T. Sullivan, W. H. Eaglstein, S. C. Davis, P. Mertz, "The pig as a model for human wound healing," *Wound Repair Regen.* **9**, 66–76 (2001).
67. C. S. Choe, J. Schleusener, J. Lademann, M. E. Darvin, "Human skin *in vivo* has a higher skin barrier function than porcine skin *ex vivo* — Comprehensive

Raman microscopic study of the stratum corneum," *J. Biophotonics* **11**, e201700355 (2018).
68. V. V. Tuchin *et al.*, "Optical clearing of skin using flashlamp-induced enhancement of epidermal permeability," *Lasers Surg. Med.* **38**, 824–836 (2006).
69. J. Schleusener, J. Lademann, M. E. Darvin, "Depth-dependent autofluorescence photobleaching using 325, 473, 633, and 785 nm of porcine ear skin *ex vivo*," *J. Biomed. Opt.* **22**, 091503 (2017).
70. F. Menges, "Spectragryph: Optical spectroscopy software: Description," https://www.effemm2.de/spectragryph/about_descr.html (2020).
71. A. Y. Sdobnov, V. V. Tuchin, J. Lademann, M. E. Darvin, "Confocal Raman microscopy supported by optical clearing treatment of the skin — influence on collagen hydration," *J. Phys. D, Appl. Phys.* **50**, 285401 (2017).
72. R. Na, I. M. Stender, M. Henriksen, H. C. Wulf, "Autofluorescence of human skin is age-related after correction for skin pigmentation and redness," *J. Invest. Dermatol.* **116**, 536–540 (2001).
73. T. Dai, B. M. Pikkula, L. V. Wang, B. Anvari, "Comparison of human skin opto-thermal response to near-infrared and visible laser irradiations: A theoretical investigation," *Phys. Med. Biol.* **49**, 4861–4877 (2004).
74. E. Guillard, A. Tfayli, M. Manfait, A. Baillet-Guffroy, "Thermal dependence of Raman descriptors of ceramides — Part II: Effect of chains lengths and head group structures," *Anal. Bioanal. Chem.* **399**, 1201–1213 (2011).
75. P. J. Caspers, G. W. Lucassen, E. A. Carter, H. A. Bruining, G. J. Puppels, "*In vivo* confocal Raman microspectroscopy of the skin: Noninvasive determination of molecular concentration profiles," *J. Invest. Dermatol.* **116**, 434–442 (2001).
76. N. Nakagawa, M. Matsumoto, S. Sakai, "*In vivo* measurement of the water content in the dermis by confocal Raman spectroscopy," *Skin Res. Technol.* **16**, 137–141 (2010).
77. T. T. Nguyen *et al.*, "Characterization of type I and IV collagens by Raman microspectroscopy: Identification of spectral markers of the dermo-epidermal junction," *J. Spectrosc. (New York)* **27**, 686183 (2012).
78. B. G. Frushour, J. L. Koenig, "Raman scattering of collagen, gelatin, and elastin," *Biopolymers* **14**, 379–391 (1975).
79. A. Nijssen *et al.*, "Discriminating basal cell carcinoma from its surrounding tissue by Raman spectroscopy," *J. Invest. Dermatol.* **119**, 64–69 (2002).
80. M. Gniadecka, H. C. Wulf, O. F. Nielsen, D. H. Christensen, J. Hercogova, "Distinctive molecular abnormalities in benign and malignant skin lesions: Studies by Raman spectroscopy," *Photochem. Photobiol.* **66**, 418–423 (1997).
81. B. H. Hokr, V. V. Yakovlev, "Raman signal enhancement via elastic light scattering," *Opt. Express* **21**, 11757 (2013).
82. P. Matousek, "Raman signal enhancement in deep spectroscopy of turbid media," *Appl. Spectrosc.* **61**, 845–854 (2007).
83. D. Oelkrug, B. Boldrini, K. Rebner, "Comparative Raman study of transparent and turbid materials: Models and experiments in the remote sensing mode," *Anal. Bioanal. Chem.* **409**, 673–681 (2017).
84. J. Jiang, R. K. Wang, "Comparing the synergistic effects of oleic acid and dimethyl sulfoxide as vehicles for optical clearing of skin tissue *in vitro*," *Phys. Med. Biol.* **49**, 5283–5294 (2004).
85. A. Liopo, R. Su, D. A. Tsyboulski, A. A. Oraevsky, "Optical clearing of skin enhanced with hyaluronic acid for increased contrast of optoacoustic imaging," *J. Biomed. Opt.* **21**, 081208 (2016).